Applied Physics Letters

Tuning the superconducting transition of $SrTiO_3$-based 2DEGs with light

Cite as: Appl. Phys. Lett. **115**, 122601 (2019); https://doi.org/10.1063/1.5119417
Submitted: 11 July 2019 . Accepted: 03 September 2019 . Published Online: 18 September 2019

D. Arnold, D. Fuchs, K. Wolff, and R. Schäfer

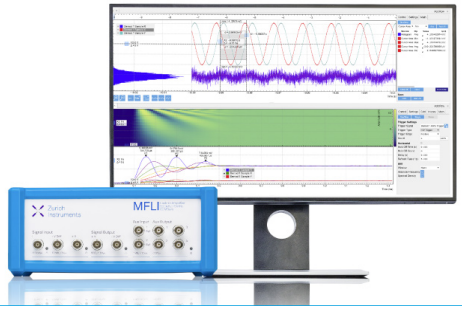

Applied Physics Letters ARTICLE scitation.org/journal/apl

Tuning the superconducting transition of $SrTiO_3$-based 2DEGs with light

Cite as: Appl. Phys. Lett. **115**, 122601 (2019); doi: 10.1063/1.5119417
Submitted: 11 July 2019 · Accepted: 3 September 2019 ·
Published Online: 18 September 2019

D. Arnold, D. Fuchs, K. Wolff, and R. Schäfer[a)]

AFFILIATIONS

Institute for Solid-State Physics, Karlsruhe Institute of Technology, D-76297 Karlsruhe, Germany

[a)]Electronic mail: roland.schaefer@kit.edu

ABSTRACT

The resistivity of the two dimensional electron gas that forms at the interface of strontium titanate with various oxides is sensitive to irradiation from visible light. In this letter, we present data on the interface between the bandgap insulators $LaAlO_3$ (LAO) and $SrTiO_3$ (STO). We operate a light emitting diode at temperatures below 1 K and utilize it to irradiate the LAO/STO interface at ultralow temperatures. On irradiation, the resistance of this system is lowered continuously by a factor of five and the resistance change is persistent at low temperatures as long as the sample is kept in the dark. This makes the characterization of transport properties in different resistive states over extended time periods possible. Our pristine sample gets superconductive below 265 mK. The transition temperature T_c shifts downward on the persistent photo-induced lowering of the resistance. The persistent photoconductance can be completely reverted by heating the structure above 10 K, in which case, T_c takes on its original value. Thus, very similar to field-effect induced changes of the electron density, irradiation at low temperatures offers a versatile tuning knob for the superconducting state of STO-based interfaces which in addition has the advantage to be nonvolatile.

A two dimensional electron gas (2DEG) develops at the interface between strontium titanate (STO) and a variety of different oxides[1–11] which offers a huge playground for many kinds of solid state phenomena (e.g., Ref. 12). Here, we focus on the low temperature transport properties which are known to be sensitive to the exposure of the 2DEG to visible light at room temperature.[13–16] Careful experiments therefore keep all samples for a considerable time in a dark environment (typically 24 h) prior to cooldown to avoid photo-induced effects which otherwise lead to relaxation effects and a drift of transport coefficients on amazingly long time scales.[13] The effect of photo induced conductivity has of course been addressed as an independent subject of interest.[17–19] It has been studied in recent years from room temperature down to $T = 1.5$ K and was found to be persistent at low temperature[18] in accordance with the aforementioned precautions taken by many researchers. The persistent charge carriers have been linked to oxygen vacancies trapped at domain boundaries which develop below the so-called antiferrodistortive transition at 105 K.[19]

A salient feature of low temperature transport of STO-based 2DEGs is superconductivity found below $T = 300$ mK.[20–22] The two dimensional confinement of the mobile carriers makes it easy to gate tune its density and in turn the conductance by the field effect.[23] For the superconducting transition temperature T_c, a dome shaped structure in the phase diagram[24,25] was found, which resembles celebrated findings in the cuprates and bulk STO. However, despite a decade of intense research, the microscopic origin of the shift in T_c with gate tuning remains controversial, as the influence and interplay of important parameters like disorder, inhomogeneity, and spin–orbit coupling are not fully understood. It is therefore desirable to find new control parameters altering the transport characteristics.[26]

In this letter, we establish persistent photoconductance as another tuning knob for the superconducting transition temperature which might give further insight into the nature of the superconducting state of the STO-based 2DEG. We operate a light emitting diode (LED) at dilution fridge temperatures. By stabilizing the temperature at $T = 500$ mK, we can monitor the resistance during irradiation by the LED and find a continuous reduction. When the LED is switched off, the resistance is constant. On the time scale of our experiment (which in some cases is extended for a period of more than a week), we could not detect any change of resistance as long as the temperature stays well below $T < 1$ K and the LED is switched off. However, the resistance change can be completely reverted by a controlled elevation of temperature to $1\,\text{K} < T < 15\,\text{K}$. The phenomenon seems to be a rather general feature and has so far been observed in $LaAlO_3$/$SrTiO_3$ (LAO/STO) heterostructures as well as in the γ–Al_2O_3/$SrTiO_3$

system. Here, we present exemplary data on an LAO/STO sample where we could reduce the resistance by a factor of five. The rate of resistance change depends on the radiant flux of the LED and is to the first order proportional to the LED current. By adjusting the radiant energy, we can set the resistance value within the total tuning range on purpose. This statement is true for both directions of resistance change. The resistance can be tuned downward by light and upward again by the elevation of temperature.

The sample has been prepared by standard pulsed laser ablation using a TiO_2-terminated (001) $SrTiO_3$ substrate and a poly crystalline $La_{0.935}Al_{1.065}O_3$ target. Film deposition was done at an oxygen pressure of $p(O_2) = 10^{-5}$ mbar onto a substrate heated to $T_{sub} = 700\,^{\circ}C$. After deposition of 150 Å LAO, the sample is rapidly cooled down to room temperature within one hour at the same partial oxygen pressure. More details on sample preparation and patterning are described elsewhere.[27,28] Electrical connections to the six arms of a Hall bar geometry are made by ultrasound wire bonding with aluminum leads.

For the purpose of irradiating the Hall bar structure at $T < 1$ K, we use a white LED (OSRAM "Golden DRAGON Plus," type LW W5AM)[29] with a radiation spectrum made up of a narrow primary emission line centered around a wavelength of 460 nm and a broad photoluminescence (PL) band with a maximal intensity around 565 nm. The diode is intended to be used in the temperature range $-40\,^{\circ}C < T < 125\,^{\circ}C$.[29] By recording the I/U characteristics in an extended temperature range [Fig. 1(a)], we gained confidence that the LED works properly even below $T < 1$ K. As expected, the forward voltage shifts to higher voltages on cooldown but this shift is rather moderate. At $T = 77$ K, we could operate the LED in an open dewar and check by visual inspection that the emitted light did not show a noticeable shift in color. However, to avoid excess heating when used at $T < 1$ K, the LED has to be operated at extremely low currents (below $I_{LED} < I_{max} = 50\,\mu A$), owing to the limited cooling power of our dilution fridge. I_{max} is by more than three orders of magnitude smaller than the minimal recommended diode current 100 mA.[29] It is not clear how efficient electrical power is converted into electromagnetic radiation in this situation.

To gain some knowledge of the efficiency, we performed the experiment sketched in Fig. 1(b) in which the LED is held at $T = 4.2$ K and a resistive thermometer is mounted at a distance of 10 mm with a sufficient thermal resistance to show a well resolved temperature rise when irradiated at low diode currents. The setup is installed on a general purpose puck of a physical property measurement system (PPMS, Quantum Design) which provides the temperature reservoir. The LED is thermally anchored thoroughly to the puck while the calibrated Cernox thermometer (R_{CX}) (Lake Shore Cryotronics, CX-1050-SD-1.4L) is supported by two thin Nylon fibers (80 μm diameter, actually dominating the thermal resistance) and electrically connected by two 30 μm thick Manganin wires of about 150 mm length. When irradiated by the LED or self-heated by a sufficiently high measurement current I_{CX}, the thermometer reaches an elevated steady state temperature T_s after a relaxation time of typically 30 min. We measure T_s as a function of I_{CX} and the diode current I_{LED}. A rise of T_s as a response to a diode current is clear evidence for the presence of an irradiance flux absorbed by R_{CX}. We take the smallest forward voltage $U_{LED} = 2.95$ V at which we could observe a temperature rise in R_{CX} (corresponding to a diode current $I_{LED} = 100$ nA) as a measure of the photon energy of the primary emission line at $T = 4.2$ K. The radiant

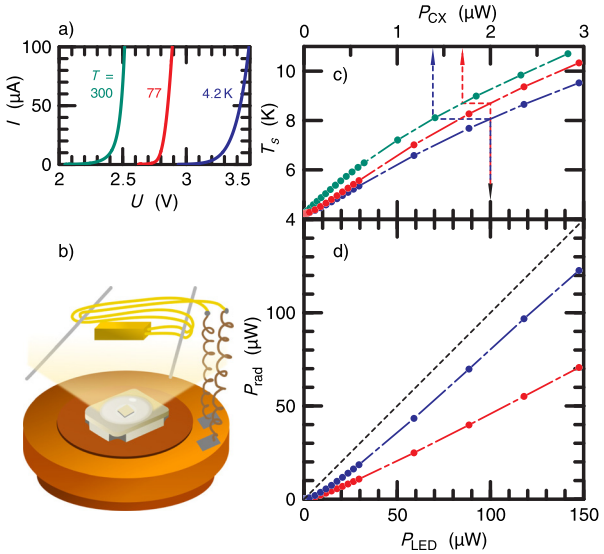

FIG. 1. (a) I/U characteristics of the light emitting diode (LED) at different temperatures. (b) Schematics of the LED calibration experiment. The radiant flux of the LED irradiates a thermometer chip (gold) supported by thin nylon fibers (gray). The leads for measuring the thermometer resistance consist of thin manganin wires. (c) Temperature of the thermometer chip as a function of electrical power dissipated by the LED (lower scale labeled P_{LED}, red and blue data). In the same diagram, the temperature elevation due to self heating of the thermometer (upper scale labeled P_{CX}, green data) is shown. With the help of this diagram, P_{LED} can be mapped onto the power dissipated by the thermometer due to light absorption. The difference between the red and the blue data is explained in the text. (d) Radiant flux of the LED as a function of effective input power at $T = 4.2$ K. The data shown in blue represent the total flux, while the data shown in red correspond to the part of the spectrum absorbed by a gold plated surface.

energy of the LED is then strictly bounded by the effective power $P_{LED} = I_{LED} \cdot 2.95$ V. In Fig. 1(c), we display T_s as a function of P_{LED} for two different runs. The blue data are recorded while the thermometer chip had its original gold plated color. It than absorbs predominantly the short wavelength photons from the main emission line while the longer wavelength PL photons are reflected. In a first run (red), the thermometer chip was covered by a black paint produced by mixing varnish (GE 7031) with carbon black. In this case, the absorption includes the long wavelength part of the spectrum resulting in an increased T_s at identical P_{LED} levels. We also recorded T_s as a function of the dissipated power P_{CX} due to self heating when I_{CX} is increased giving identical results in both runs (green). As indicated by the arrow headed lines in Fig. 1(c), we can relate P_{LED} to P_{CX} which gives a measure for the irradiance flux absorbed by R_{CX}. Finally, a geometry factor f can be deduced relating the radiant power of the LED to the irradiance flux received by the surface of R_{CX}. Actually, uncertainties in the latter quantity dominate the systematic error of this experiment and limit the accuracy of the final result presented in Fig. 1(d) to about 20%. In this figure, f is taken into account to calculate the radiant flux P_{rad} which is plotted as a function of P_{LED}. The black dashed line represents the theoretical limit, while the blue and red data represent the fraction of radiant flux dissipated by a black and gold plated absorber, respectively. Figure 1(d) reports an amazingly high efficiency of the LED at 4.2 K. The total radiant intensity of our light source is about

500 nW/(μA sr) · I_{LED} in the forward direction. The persistent photoconductance discussed in the rest of this letter is most likely caused by the short wavelength part of the spectrum (this is the radiation absorbed by the gold plated R_{CX}). Its radiant intensity is found to be 300 nW/(μA sr) · I_{LED}.

After characterizing the light source, we describe in the rest of this letter our main experiment sketched in Fig. 2(a) which is installed in a commercial dilution refrigerator (Oxford Instruments, MX250). The Hall bar structured sample is thermally anchored at a sample stage. The temperature of the sample stage T_{ss} is regulated by a proportional-integral-derivative (PID) controller using a resistor chip R_h as heater and can be varied in the range 12 mK < T_{ss} <2 K. Reaching higher temperatures is difficult without removing the ^{3}He/^{4}He insert from the liquid helium bath. Nevertheless, we managed to heat our sample to about $T_{ss} \approx 10$ K by running our insert in a special operation mode (see below). In this case, the temperature is only weakly controlled. The sheet resistance $R_\square$ of the sample is measured with a lock-in technique: an ac current of amplitude $I_{AC} = 9$ nA which is reduced to $I_{AC} = 2$ nA for temperature dependent $R_\square(T)$ measurements is sourced to the central strip of the Hall bar structure. The resulting voltage drop U_{AC} over two side terminals is amplified by a home-build amplifier and measured by the lock-in amplifier (Signal Recovery, Model 7265 DSP). The length between the voltage terminals equals 12 times the width of the central strip and $R_\square = U_{AC}/(12 I_{AC})$. We carefully checked that we stay in the linear regime of the current voltage characteristics which made it necessary to reduce the measurement current close the superconducting transition. The Hall resistance is recorded in fields up to 8 T by measuring the voltage across two terminals opposite to each other and supplies us with information on the sheet carrier concentration.

The LED light source is mounted at ~10 mm distance from the sample. LED currents of 100 nA < I_{LED} < 50 μA are supplied by a source/measure unit (Keithley Model 2400) via superconducting leads. Operating the LED at higher power leads to a heat burden of the sample stage. In principle, I_{LED} could replace the current sourced to R_h in the PID regulation circuit. For the experiments described here, we use R_h for temperature control and always stabilize the stage at $T_{ss} = 500$ mK before slowly turning on I_{LED}. The PID regulation reacts to the increasing P_{LED} by reducing the current sourced to R_h keeping T_{ss} almost constant ($|\Delta T_{ss}| < 5$ mK). At $I_{LED} = 50\,\mu$A, the current through R_h is set to zero by the PID circuitry and heating is solely due to the dissipation of the LED.

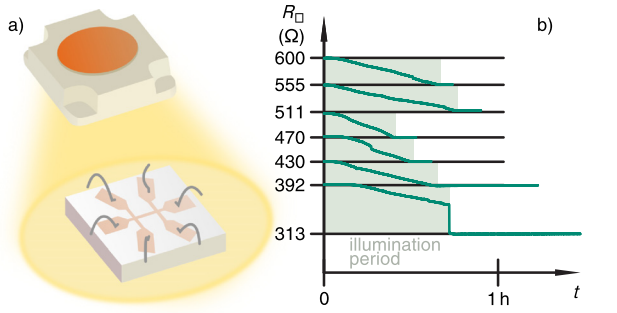

FIG. 2. (a) Schematics of the LAO/STO sample structured in Hall bar geometry and irradiated by an LED. The setup is operated in a dilution refrigerator at $T \leq 500$ mK. (b) Sheet resistance $R_\square$ vs time at $T = 500$ mK. During light exposure (period marked in green), $R_\square$ drops continuously while it stays constant when the LED is switched off. In some instances, $R_\square$ displays a sudden jump during illumination. One such instance can be seen between 392 Ω and 313 Ω.

A constant T_{ss} does not automatically guarantee a constant temperature of the 2DEG at the LAO/STO interface of our sample. Because of the positive temperature coefficient of $R_\square$ at $T = 500$ mK, an increase in the temperature of the 2DEG as a response to irradiation would result in an increase in $R_\square$. In contrast, light exposure at a constant T_{ss} leads to a decrease in $R_\square$. It alters the resistive state of our sample and this alteration cannot be attributed to heating. Examples are given in Fig. 2(b). Within the green marked period, the sample was illuminated by setting I_{LED} to values between 1 and 5 μA. During illumination, $R_\square$ decreases as a function of time. As soon as we turn off I_{LED}, $R_\square$ stabilizes at its reduced, momentary value. As long as the LED remains switched off and $T_{ss} \lesssim 1$ K, $R_\square$ is a function of magnetic field and temperature only and does not change over time. Initially, $R_{res} \equiv R_\square(T = 500\,\text{mK})$ was found to be $R_{res} = 600\,\Omega$. Subsequently, we altered the resistive state of our sample in steps of about 42 Ω. In Fig. 3(a) where R_{res} is displayed as a function of the radiant exposure D, this first series is represented by red symbols. The abscissa in this figure is deduced from $\int I_{LED} dt$ with the help of the LED calibration presented earlier and corresponds to the total radiant energy per unit area irradiated to the sample by the LED in the short wavelength part of the spectrum.[30] Most likely, only high energetic photons are responsible for the persistent conductance effect.[19] However, we do not have further evidence for this statement and additional experiments with monochromatic LEDs are required for proof. The total radiant exposure over all wavelengths is 70% larger.

Light exposure leads to a persistent reduction of $R_\square$. However, the resistance change can be reverted by heating the sample to T_{ss} > 1 K. The rate of resistance "increase" depends in this case on the temperature and speeds up considerably above $T > 4.2$ K. Unfortunately, it is almost impossible to regulate temperatures in the regime $T > 2$ K in our dilution fridge. While we could reach temperatures of the order 12 K > T > 10 K by thermally isolating[31] and heating the mixing chamber, this temperature is only weakly controlled. Nevertheless, we could convince ourselves, that R_{res} measured after cooling the sample down again after heat treatment depends strongly on the peak temperature reached during the procedure and only weakly on the time period it lasts. The minimal resistance $R_{res} = 120$ Ω we could achieve by irradiation is in this respect related to the temperature $T = 500$ mK at which it is measured and lower resistive states might in principle be reached by irradiation at lower temperatures but relax back to $R_{res} = 120\,\Omega$ if the sample is heated to $T = 500$ mK.

Afterward, we were able to increase R_{res} in small steps by controlled heating. Again, at a low temperature and while the LED is switched off, $R_\square$ is a function of magnetic field and temperature only and is absolutely stable over time. By heating the sample to $T_{ss} \approx 12$ K, we could reach resistance states with an even slightly higher $R_{res} = 675$ Ω than the initial value of 600 Ω. Subsequently, we lowered the resistance again by utilizing the LED. This second run is shown as green symbols in Fig. 3(a) giving consistent results. Analyzing the dependence of R_{res} (D) gives the empirical results shown as black lines in Fig. 3(a). The experimental data are well described by

$$R_{res}(D) = R_{ini} - \Delta R \cdot L_D, \quad L_D \equiv 10 \log_{10}\left(\frac{D}{1(\text{mJ cm}^{-2})}\right) \text{dB},$$

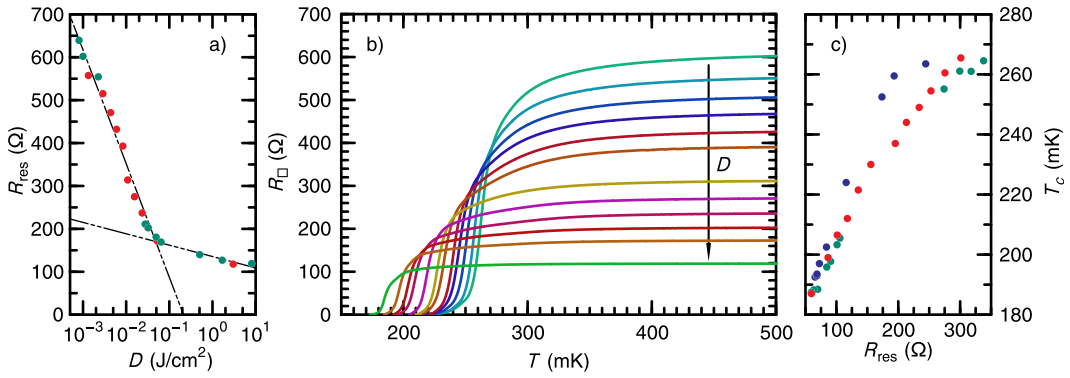

FIG. 3. (a) Residual sheet resistance $R_{res} = R_\square(500\,\text{mK})$ as a function of radiant exposure D in the short wavelength part of the LED spectrum. The red dots correspond to the irradiance sequence shown in (b). The green dots represent the result of a second sequence recorded after a temperature induced reset of R_{res}. The black lines are a guide to the eye explained further in the text. (b) Sheet resistance $R_\square$ as a function of temperature T for various residual resistances R_{res}. The shown curves are measured successively while R_{res} has been reduced in between by a controlled irradiation. The LED is switched off during the measurements. (c) Superconducting transition temperature T_c as a function of R_{res}. The red and green symbols as in (a), while the blue dots are the results obtained during the temperature controlled resistance increase.

with different initial resistance values ($R_{ini} = 617\,\Omega, 215\,\Omega$) and slopes ($\Delta R = 26.5\,\Omega/\text{dB}, 2.65\,\Omega/\text{dB}$) at lower and higher doses, respectively.

In Fig. 3(b), we present $R_\square(T)$ in the different persistent resistance states of the first light induced reduction series [corresponding to the red symbols in Fig. 3(a)]. During these measurements, $I_{LED} = 0$. All curves have been measured repeatedly with falling as well as rising temperatures and lead to reproducible results which do not differ within the line thickness in the figure. The curves in Fig. 3(b) display superconductivity at low temperatures with a transition temperature T_c which shifts downward with decreasing R_{res}. This effect is summarized in Fig. 3(c) where T_c was estimated as the temperature, where $R_\square(T_c) = R_{res}/2$. In the initial sequence of resistance reduction by illumination, T_c decreased monotonically from $T_c = 265$ mK down to $T_c = 187$ mK. Also included are results from the stepwise increase in R_{res} due to controlled heating. Measurements of $R_\square(T)$ in different resistive states lead to the blue dots in Fig. 3(c). $R_{res} = 490\,\Omega$ could be reached easily by heating the sample to $T \approx 11$ K. In this state, T_c fully recovers to $T_c = 264$ mK. We then kept the sample for an extended period of several days at $T \lesssim 12$ K and could increase R_{res} even further ($R_{res} = 675\,\Omega$). However, this had only a minor effect on T_c. The final illumination sequence with falling R_{res} is shown as green symbols and shows the reproducibility of our finding.

The observed reduction of T_c with decreasing R_{res} is typical for the so-called over-doped regime, and indeed taking the resistance range of our experiment ($120\,\Omega < R_\square < 600\,\Omega$) into account, this finding is in accord with the published data[24,25] on field effect tuned resistivities. Our Hall resistivity measurements show a zero field slope ($R_H = 43\,\Omega/\text{T}$) which is almost independent of R_{res} in accordance with the data presented in Ref. 32. Within the limited field range of our magnet ($\pm$ 8 T), we only see slight nonlinearities at larger fields which get more pronounced as R_{res} is lowered. These nonlinearities are evidence that more than one band contributes to electrical transport at low temperatures and makes the correspondence between the carrier concentration and Hall effect rather complicated. Measurements at higher fields would be desirable and might allow a meaningful fitting of the Hall data with a multiband model.

For now, the microscopic mechanism of light induced changes is absolutely unclear. Findings by other authors[19] differ in subtle details. We completely revert the photo-induced transport changes at comparatively low temperatures ($T \approx 12$ K), while in Ref. 19, a crossing of the antiferro-distortive transition of STO at $T \approx 105$ K seems to be necessary to revert persistence in photo-conductance. The difference might route in a smaller photon energy in our case. The LED radiates at $h\nu \lesssim 2.95$ eV, which is of the order but considerably smaller than the bandgap of STO ($E_{gap} = 3.2$ eV). Other experiments on persistent photo-conductance use UV light above the gap energy.

In summary, we present a setup to tune the transport behavior of STO-based interfaces at low temperatures with light. The radiant intensity of a LED was calibrated at $T = 4.2$ K as a function of current and utilized as the light source below 1 K. By adjusting the radiant energy, we were able to tune the residual sheet resistance R_{res} at 500 mK, while simultaneously changing the superconducting transition temperature T_c. We reported a monotonous behavior of T_c vs R_{res} for different resistive states. To reverse the altered state, we used heat treatment up to 12 K. By using visible light at low temperatures, we introduced a nonvolatile tuning parameter on the superconductivity of the STO-based interfaces.

This paper was supported by the Deutsche Forschungsgemeinschaft (Grant Nos. SCHA 658/2-1 and FU 457/2-1). We thank K. Grube for the fruitful discussion.

REFERENCES

[1]A. Ohtomo and H. Y. Hwang, "A high-mobility electron gas at the $LaAlO_3$/$SrTiO_3$ heterointerface," Nature **427**, 423–426 (2004).
[2]S. S. A. Seo, W. S. Choi, H. N. Lee, L. Yu, K. W. Kim, C. Bernhard, and T. W. Noh, "Optical study of the free-carrier response of $LaTiO_3$/$SrTiO_3$ superlattices," Phys. Rev. Lett. **99**, 266801 (2007).
[3]P. Perna, D. Maccariello, M. Radovic, U. Scotti di Uccio, I. Pallecchi, M. Codda, D. Marré, C. Cantoni, J. Gazquez, M. Varela, S. J. Pennycook, and F. M. Granozio, "Conducting interfaces between band insulating oxides: The $LaGaO_3$/$SrTiO_3$ heterostructure," Appl. Phys. Lett. **97**, 152111 (2010).
[4]P. Moetakef, T. A. Cain, D. G. Ouellette, J. Y. Zhang, D. O. Klenov, A. Janotti, C. G. Van de Walle, S. Rajan, S. J. Allen, and S. Stemmer, "Electrostatic carrier doping of $GdTiO_3$/$SrTiO_3$ interfaces," Appl. Phys. Lett. **99**, 232116 (2011).

[5]D. F. Li, Y. Wang, and J. Y. Dai, "Tunable electronic transport properties of $DyScO_3/SrTiO_3$ polar heterointerface," Appl. Phys. Lett. **98**, 122108 (2011).
[6]S. W. Lee, Y. Liu, J. Heo, and R. G. Gordon, "Creation and control of two-dimensional electron gas using Al-based amorphous oxides/$SrTiO_3$ heterostructures grown by atomic layer deposition," Nano Lett. **12**, 4775–4783 (2012).
[7]C. He, T. D. Sanders, M. T. Gray, F. J. Wong, V. V. Mehta, and Y. Suzuki, "Metal-insulator transitions in epitaxial $LaVO_3$ and $LaTiO_3$ films," Phys. Rev. B **86**, 081401 (2012).
[8]A. Annadi, A. Putra, Z. Q. Liu, X. Wang, K. Gopinadhan, Z. Huang, S. Dhar, T. Venkatesan, and Ariando, "Electronic correlation and strain effects at the interfaces between polar and nonpolar complex oxides," Phys. Rev. B **86**, 085450 (2012).
[9]C. Li, Q. Xu, Z. Wen, S. Zhang, A. Li, and D. Wu, "The metallic interface between insulating $NdGaO_3$ and $SrTiO_3$ perovskites," Appl. Phys. Lett. **103**, 201602 (2013).
[10]Y. Z. Chen, N. Bovet, F. Trier, D. V. Christensen, F. M. Qu, N. H. Andersen, T. Kasama, W. Zhang, R. Giraud, J. Dufouleur, T. S. Jespersen, J. R. Sun, A. Smith, J. Nygård, L. Lu, B. Büchner, B. G. Shen, S. Linderoth, and N. Pryds, "A high-mobility two-dimensional electron gas at the spinel/perovskite interface of γ-$Al_2O_3/SrTiO_3$," Nat. Commun. **4**, 1371 (2013).
[11]P. Xu, D. Phelan, J. Seok Jeong, K. Andre Mkhoyan, and B. Jalan, "Stoichiometry-driven metal-to-insulator transition in $NdTiO_3/SrTiO_3$ heterostructures," Appl. Phys. Lett. **104**, 082109 (2014).
[12]P. Zubko, S. Gariglio, M. Gabay, P. Ghosez, and J.-M. Triscone, "Interface physics in complex oxide heterostructures," Annu. Rev. Condens. Matter Phys. **2**, 141–165 (2011).
[13]M. Huijben, G. Rijnders, D. H. A. Blank, S. Bals, S. V. Aert, J. Verbeeck, G. V. Tendeloo, A. Brinkman, and H. Hilgenkamp, "Electronically coupled complementary interfaces between perovskite band insulators," Nat. Mater. **5**, 556–560 (2006).
[14]Y. Lei, Y. Li, Y. Z. Chen, Y. W. Xie, Y. S. Chen, S. H. Wang, J. Wang, B. G. Shen, N. Pryds, H. Y. Hwang, and J. R. Sun, "Visible-light-enhanced gating effect at the $LaAlO_3/SrTiO_3$ interface," Nat. Commun. **5**, 5554 (2014).
[15]Y. Li, Y. Lei, B. G. Shen, and J. R. Sun, "Visible-light-accelerated oxygen vacancy migration in strontium titanate," Sci. Rep. **5**, 14576 (2015).
[16]A. Tebano, E. Fabbri, D. Pergolesi, G. Balestrino, and E. Traversa, "Room-temperature giant persistent photoconductivity in $SrTiO_3/LaAlO_3$ heterostructures," ACS Nano **6**, 1278–1283 (2012).
[17]Z. Yang, Y. Chen, H. Zhang, H. Huang, S. Wang, S. Wang, B. Shen, and J. Sun, "Joint effect of gate bias and light illumination on metallic $LaAlO_3/SrTiO_3$ interface," Appl. Phys. Lett. **111**, 231602 (2017).
[18]L. Cheng, L. Wei, H. Liang, Y. Yan, G. Cheng, M. Lv, T. Lin, T. Kang, G. Yu, J. Chu, Z. Zhang, and C. Zeng, "Optical manipulation of rashba spin–orbit coupling at $SrTiO_3$-based oxide interfaces," Nano Lett. **17**, 6534–6539 (2017).
[19]M. Yazdi-Rizi, P. Marsik, B. P. P. Mallett, K. Sen, A. Cerreta, A. Dubroka, M. Scigaj, F. Sánchez, G. Herranz, and C. Bernhard, "Infrared ellipsometry study of photogenerated charge carriers at the (001) and (110) surfaces of $SrTio_3$ crystals and at the interface of the corresponding $LaAlO_3/SrTiO_3$ heterostructures," Phys. Rev. B **95**, 195107 (2017).
[20]N. Reyren, S. Thiel, A. D. Caviglia, L. F. Kourkoutis, G. Hammerl, C. Richter, C. W. Schneider, T. Kopp, A.-S. Rüetschi, D. Jaccard, M. Gabay, D. A. Muller, J.-M. Triscone, and J. Mannhart, "Superconducting interfaces between insulating oxides," Science **317**, 1196–1199 (2007).
[21]J. Biscaras, N. Bergeal, A. Kushwaha, T. Wolf, A. Rastogi, R. C. Budhani, and J. Lesueur, "Two-dimensional superconductivity at a Mott insulator/band insulator interface $LaTiO_3/SrTiO_3$," Nat. Commun. **1**, 89 (2010).
[22]D. Fuchs, R. Schäfer, A. Sleem, R. Schneider, R. Thelen, and H. von Löhneysen, "Two-dimensional superconductivity between $SrTiO_3$ and amorphous Al_2O_3," Appl. Phys. Lett. **105**, 092602 (2014).
[23]S. Thiel, G. Hammerl, A. Schmehl, C. W. Schneider, and J. Mannhart, "Tunable quasi-two-dimensional electron gases in oxide heterostructures," Science **313**, 1942–1945 (2006).
[24]A. D. Caviglia, S. Gariglio, N. Reyren, D. Jaccard, T. Schneider, M. Gabay, S. Thiel, G. Hammerl, J. Mannhart, and J.-M. Triscone, "Electric field control of the $LaAlO_3/SrTiO_3$ interface ground state," Nature **456**, 624–627 (2008).
[25]S. Gariglio, M. Gabay, and J.-M. Triscone, "Research update: Conductivity and beyond at the $LaAlO_3/SrTiO_3$ interface," APL Mater. **4**, 060701 (2016).
[26]D. Fuchs, A. Sleem, R. Schäfer, A. G. Zaitsev, M. Meffert, D. Gerthsen, R. Schneider, and H. van Löhneysen, "Incipient localization of charge carriers in the two-dimensional electron system in $LaAlO_3/SrTiO_3$ under hydrostatic pressure," Phys. Rev. B **92**, 155313 (2015).
[27]D. Fuchs, K. Wolff, R. Schäfer, R. Thelen, M. Le Tacon, and R. Schneider, "Patterning of two-dimensional electron systems in $SrTiO_3$ based heterostructures using a CeO_2 template," AIP Adv. **7**, 056410 (2017).
[28]K. Wolff, R. Eder, R. Schäfer, R. Schneider, and D. Fuchs, "Anisotropic electronic transport and rashba effect of the two-dimensional electron system in (110) $SrTiO_3$-based heterostructures," Phys. Rev. B **98**, 125122 (2018).
[29]Golden DRAGON Plus, Osram Opto Semiconductors GmbH, 2010.
[30]The calibration is performed at $T = 4.2$ K, while the illumination takes place at a considerably lower temperature. We do not see a significant change of the diode characteristic when the temperature is lowered from $T = 4.2$ K. It is quite likely that the temperature of the light emitting layer is elevated during operation and is not determined by the mixing chamber setting below $T \lesssim 1$ K. For this reason, we are confident that the calibration of a diode at 4.2 K correctly describes the behavior at dilution fridge temperatures. In any case, $\int I_{LED} dt$ is proportional to the real dose. A change of the constant of proportionality leads to a small horizontal shift in Fig. 3(a) only.
[31]This is done by pumping out the 3He/4He-mixture. An absorption pump at the condenser is still kept at $T = 1.7$ K to maintain good isolation from the 4He bath. This actually limits the maximal sample temperature we can reach by heating the mixing chamber.
[32]A. Joshua, S. Pecker, J. Ruhman, E. Altman, and S. Ilani, "A universal critical density underlying the physics of electrons at the $LaAlO_3/SrTiO_3$ interface," Nat. Commun. **3**, 1129 (2012).